Eur. Phys. J. B **38**, 93–98 (2004)
DOI: 10.1140/epjb/e2004-00103-4

THE EUROPEAN PHYSICAL JOURNAL B

Noise correction for roughening analysis of magnetic flux profiles in $YBa_2Cu_3O_{7-x}$

M.S. Welling[a], C.M. Aegerter, and R.J. Wijngaarden

Division of Physics and Astronomy, Faculty of Sciences, Vrije Universiteit, De Boelelaan 1081, 1081HV Amsterdam, The Netherlands

Received 1st July 2003 / Received in final form 9 February 2004
Published online 20 April 2004 –

Abstract. The presence of experimental noise may greatly reduce the accuracy of experimentally determined growth and roughness exponents, which characterize a growing self-affine interface. A separate determination of the experimental noise enables a straightforward correction, which we demonstrate on experiments on the roughening of magnetic flux profiles in the critical state of $YBa_2Cu_3O_{7-x}$ thin films. After noise correction, we find that the magnetic field *profile* is characterized by a roughness exponent $\alpha = 0.75(6)$. The growth exponent of the profiles is $\beta = 0.7(1)$.

PACS. 05.65.+b Self-organized systems – 45.70.-n Granular systems

1 Introduction

Kinetic roughening of interfaces ideally produces self-affine objects, which are characterized by power law scaling exponents. Such roughening behavior is commonplace in nature and can be seen in many diverse experimental systems, such as the growth of bacterial colonies [1], fluid flow in porous media [2–4], the tearing [5] and burning [6–8] of paper, as well as in mountain ranges [9] and granular piles [10,11]. Experimentally, however, there are sometimes difficulties in obtaining reliable estimates of the characteristic exponents. One major problem is the presence of noise in the experimental data. The noise dominates on small length scales, destroying power law scaling due to the introduction of an 'intrinsic width' [12–14]. In experimental systems, where power law scaling is observed over a limited number of decades, this intrinsic width influences the determination of the exponents [14]. For this reason, ideally, one should correct for the noise. In this paper we demonstrate that this is feasible for any system where one can experimentally determine the noise properties. We apply our noise correction method to the study of roughening of magnetic flux *profiles* in the critical state of $YBa_2Cu_3O_{7-x}$ thin films.

The outline of this paper is as follows. In Section 2, the experimental set-up is introduced, including a discussion of the origins of noise together with an error propagation analysis. The analysis methods used to characterize the self-affine behavior are discussed in Section 3. We show how noise changes the correlation functions which characterize the power law scaling behavior. Relations are presented which enable the removal of the influence of noise. We validate this procedure in Section 4, applying it to interfaces generated by a numerical random walk model, where the power law scaling properties are well known analytically. The results of the noise correction on the self-affine analysis of our experimental magnetic flux profiles are presented in Section 5. Section 6, summarizes the results and puts them into a broader perspective.

2 Experimental details

In the magneto-optical (MO) experiments presented here, the local magnetic field immediately above the superconducting sample is measured. This is achieved by detecting the polarization change in a Bi-doped Yttrium Iron Garnet (YIG) film [15], with in-plane anisotropy and which exhibits a large Faraday effect (typically 0.07 deg/mT). This "indicator" is mounted on top of the sample, which is a $YBa_2Cu_3O_{7-x}$ (YBCO) superconducting thin film on a $NdGaO_3$ substrate. The film was made by Pulsed Laser Deposition (PLD) [16] and has a strip geometry with an aspect ratio of 1:9, the long edge having a dimension of 8.1 mm. The sample thickness is 80 nm. Only the middle part of the strip is used in order to eliminate the effect of the corners on the shape of the flux landscape.

The assembly consisting of sample and indicator is mounted in a specially built cryogenic polarization microscope, which fits into the variable temperature insert of an Oxford instruments 1 T magnet system. The applied magnetic field is perpendicular to the sample and indicator surface. Experiments are performed at 4.2 K, after zero field cooling (ZFC). The applied magnetic field is increased from 0 mT to 17 mT in steps of 50 μT, using

[a] e-mail: welling@nat.vu.nl

a constant sweep rate of 1 mT/s in between steps. After every field step, the flux distribution in the sample is relaxed for 10 seconds after which an image is acquired. The pictures are taken with a charge-coupled device camera using an exposure time of 500 ms. The spatial resolution is such that 1 pixel corresponds to 1.4 μm. The experiment was repeated five times (including the ZFC procedure) to improve statistics.

Next, we discuss the origin of noise in the experimental system and its propagation in the data. Using a newly developed MO image lock-in amplifier (MO-ILIA) [17], the Faraday angle ϕ, which is proportional to the local magnetic field, is measured directly. This technique is a considerable improvement compared to conventional magneto-optics due to the intrinsic linearity in field, the direct measurement of the sign of the field, and the improved sensitivity at small magnetic fields. In the MO-ILIA, a Faraday angle image is calculated from the measured intensities of three images (a, b, and c) taken at different angles between polarizer and analyzer (α, 0, $-\alpha$ with respect to crossed position). For small ϕ and α, the intensities in these images are given by

$$a = I(\phi + \alpha)^2 + K \tag{1}$$

$$b = I(\phi)^2 + K \tag{2}$$

$$c = I(\phi - \alpha)^2 + K \tag{3}$$

where K is an offset due to stray light, imperfect polarizers and camera offset. I is the incident illumination intensity. The Faraday angle ϕ is found from the images a, b, and c using

$$\phi = \frac{\alpha}{2}\frac{a-c}{\langle a + c - 2b\rangle_N} = \frac{a-c}{4\alpha I}. \tag{4}$$

This calculation is applied to each pixel separately. As indicated in equation (4), the illumination intensity is estimated using $I = \langle a + c - 2b\rangle_N/(2\alpha^2)$, where $\langle..\rangle_N$ denotes averaging over N consecutive images, which is allowed since the illumination intensity is constant during the whole experiment. If noise is present in the a, b, and c images, this averaging significantly decreases the noise in ϕ.

Since the main source of noise in the acquired a, b, and c images is photon counting noise, we assume for the following error propagation analysis that the noise in a, b, and c is proportional to the square root of the image intensity (e.g. $\delta a = \sqrt{a}$). A simple error propagation analysis shows that the noise amplitude $\delta\phi$ in the calculated Faraday angle ϕ is:

$$\sigma = \delta\phi = \frac{1}{\sqrt{8I}}\sqrt{1 + \left(1 + \frac{4}{N}\right)\frac{\phi^2}{\alpha^2} + \frac{K}{I\alpha^2}\left(1 + \frac{12\phi^2}{N\alpha^2}\right) + \frac{12\phi^4}{N\alpha^4}} \tag{5}$$

which for $N \longrightarrow \infty$ reduces to

$$\sigma = \delta\phi = \frac{1}{\sqrt{8I}}\sqrt{1 + \left(\frac{\phi}{\alpha}\right)^2 + \frac{K}{I\alpha^2}}. \tag{6}$$

Note that for later reference we define σ as the strength of the noise. For $N = 100$ the difference in $\delta\phi$ calculated by equation (6) or equation (5) is less than 1% for typical experimental values of I, K, α, and ϕ. As follows directly from equation (6), reduction of the noise is possible by increasing I. However, in practice I cannot be increased at will since we use a 12 bit camera and the intensity of the measured images a, b, and c is limited by the maximum camera illumination. We optimize the illumination intensity of images a and c such that the camera doesn't saturate for any measured ϕ value. This optimization process maximizes I. Note that the first and third term in equation (6) are independent of ϕ, thus can be determined if ϕ is zero as discussed later on.

3 Analysis methods

The experiment is carried out after ZFC for increasing external field values. As an example, the part of the sample used for analysis is shown in Figure 1 at 15 mT external field as a 3-dimensional image where height is proportional to local magnetic field. The edge of the sample is the high intensity ridge. One can clearly identify an overall surface reminiscent of a granular pile. In order to obtain profiles from the flux distribution in the sample we first determine the position of the front of the penetrating flux (the white line in Fig. 1). The front is defined as the position where the local field equals three times the standard deviation of the noise in the field free Meissner region. The flux profile is defined starting at the front and going backwards, 128 pixels towards the sample edge in a direction perpendicular to the sample edge. Thus the profiles are connected to the fronts and mimic the behavior of a statistically stationary state, where the *'mass of the pile'* is constant in time.

To enable a more straightforward discussion of the influence of experimental noise, we write the profile $B_z(x, y)$ in terms of the Faraday angle (we define v as the corresponding proportionality constant). In addition, for the roughening and growth analysis, we remove the average slope, which results in the definition of a slope-free rescaled profile as $b(x, y) = v\,(B_z(x, y) - \langle B_z(x, y, t)\rangle_{y,t})$. Here $\langle B_z(x, y, t)\rangle_{y,t}$ is the average profile over a whole experiment consisting of 128 images obtained at different times t for different external fields. Since we want to study the *fluctuations* in the slope-free profiles we remove this average profile. In every image there are 200 profiles (at 200 different y values). Since the y index only labels a particular profile, we drop that index in the analysis below. With five different experiments of 128 images each, there are $5 \times\ 128 \times\ 200 \simeq\ 10^5$ profiles for the analysis.

Since the profiles are clearly not smooth, a self-affine analysis is performed in terms of a roughness exponent α and a growth exponent β. The roughness of an interface is classically [14] quantified by its width $w(L, t)$ defined as

$$w(L, t) = \langle(b(x, t) - \langle b(x, t)\rangle_L)^2\rangle^{1/2}, \tag{7}$$

where $\langle.\rangle_L$ is a spatial average over x in a window of length L on the interface. The outer brackets denote an

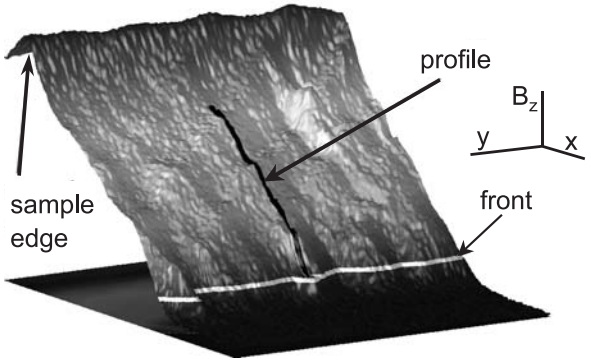

Fig. 1. A 3-dimensional plot of a magneto-optical image of the vortex landscape in an $YBa_2Cu_3O_{7-x}$ thin film at an applied field of 15 mT (height is proportional to local magnetic field). Indicated in black is the profile as defined by moving away from the front (white contour) towards the sample edge for 128 pixels. The edge of the sample is clearly visible as the high intensity ridge.

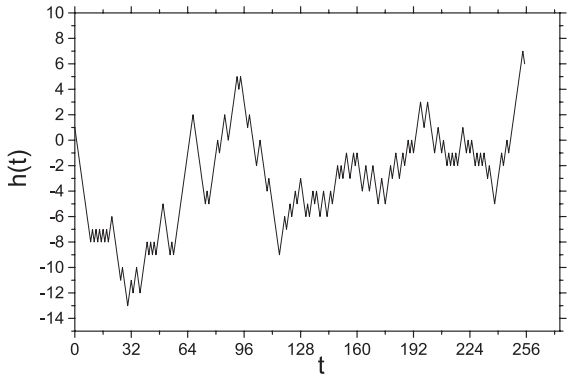

Fig. 2. A typical example of the random walk trajectory used as an ideal self-affine interface. The length of the simulation is 256 pixels. In total 50000 such random walks were analyzed.

ensemble average (i.e. over y, the 5 experiments and the 128 images per experiment). For a self-affine interface, the width grows with time as a power law: $w(t) \propto t^{\beta}$ until the correlation length becomes comparable to the system size and saturation occurs; β is called the growth exponent. The saturation value w_{sat} grows with the window size L as a power law: $w_{sat} \propto L^{\alpha}$, where α is the roughness exponent. In the experiments presented here, a *measured* magnetic field profile $B_z(x)$ is not only due to the magnetic field of the sample but also due to a noise contribution η with width σ as given by equation (5), thus:

$$b(x) = h(x) + \eta(x). \tag{8}$$

Here $h(x)$ is the true slope-free profile and $b(x)$ is the measured noisy slope-free profile. Due to the presence of noise we do not find directly the true width if we apply equation (7) to the measured interface. If the noise is not correlated to the height, the measured width of an interface w_b contains a noise contribution according to:

$$w_b^2 = w_h^2 + \sigma^2. \tag{9}$$

Hence the true width w_h can be calculated from the measured width w_b using the experimentally determined σ, which is often called [14] the *intrinsic width*. In general, however, the width of the interface yields not the most accurate determination of the exponents. An alternative is the two-point correlation function $C(x,t)$, which scales as the width for a self-affine interface [14]. The correlation function is defined by

$$C(x,t) = \left(\langle (b(\xi,\tau) - b(x+\xi, t+\tau))^2 \rangle_{\xi,\tau}\right)^{1/2}. \tag{10}$$

Here spatial or temporal averaging is denoted by $\langle .. \rangle_{\xi,\tau}$. Its power law scaling behavior is such that $C(x,0) \propto x^{\alpha}$ and $C(0,t) \propto t^{\beta}$. Due to averaging over many data points, especially at small scales, the exponents α and β can be determined more accurately. At large length or long time scales $C(x,t)$ is averaged only over a few points, decreasing its accuracy.

As mentioned above, $C(x,0)$ and $C(0,t)$ are calculated from the ensemble average over 10^5 profiles.

For noisy data, a correction similar to that of the width is easily derived for the two-point correlation function. Inserting equation (8) into equation (10), gives

$$C_b^2 = C_h^2 + 2\sigma^2, \tag{11}$$

which again allows to calculate the true correlation function C_h from the correlation function C_b as calculated from noisy data, once σ is known. Note that σ represents the *noise average along the profile*. Thus with experimental knowledge of the noise we may again find the true correlation function. We will now validate the ideas presented above using a random walk simulation.

4 Validation of the noise removal method using simulated data

It is well known that a one-dimensional random walk $h(t)$ produces a self-affine curve as a function of time with width $w(h(t)) \propto t^{0.5}$. To compare the methods of noise correction discussed in the previous section, we apply these to a number of random walk profiles (50000) comparable to the number of magnetic field profiles measured in our MO experiments. An example of such an 'interface' can be seen in Figure 2. The two-point correlation function of these random walks is shown in Figure 3. The exponent given by the slope of the double-logarithmic plot in Figure 3 is 0.50(1) over more than 2 orders of magnitude in excellent agreement with the analytical result.

To test our method, we first add Gaussian noise with zero mean and width σ to the random walks. In Figure 4, the correlation functions are shown for the same simulations as Figure 3, however with 25% noise added ($\sigma/\sqrt{256} = 25\%$). The uncorrected correlation function (open circles) shows a clear flattening-off at small time scales. Even at long time scales the exponent of 0.5 is never reached, indicating the real need for removal of the

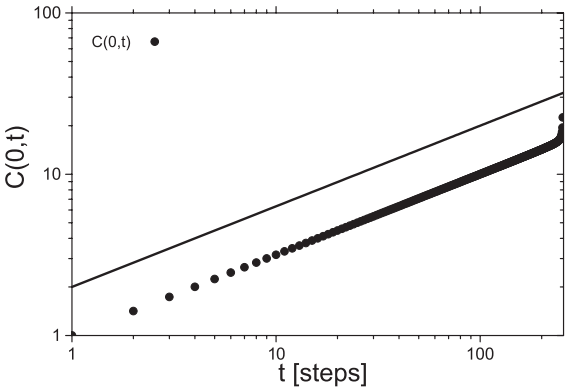

Fig. 3. The two-point correlation function $C(0,t)$ (filled circles) averaged over all simulated random walks. The exponent of the simulation (0.50(1)) is in nice agreement with the analytical result (0.5), indicated by the line.

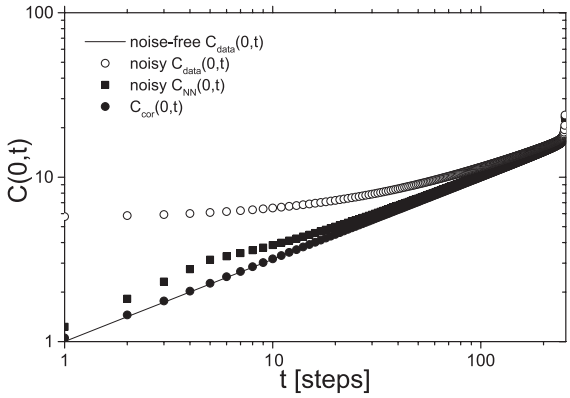

Fig. 4. Two-point correlation functions of the random walks with and without added noise. Indicated by the open circles are the results for the noisy random walks $C_{data}(0,t)$. A determination of the exponent gives a too low value, $\alpha = 0.30(5)$, in the "linear" region. The result $C_{NN}(0,t)$ for adjacent averaging (see text) is shown with filled squares. Here, the averaging introduces correlations and a too high exponent at small time scales. Furthermore the exponent obtained at longer times is too low, $\alpha = 0.43(3)$. The filled circles show $C_{cor}(0,t)$, i.e. with the known noise removed from the correlation function according to equation (11). Here the analytic result is recovered, $\alpha = 0.50(2)$. Note also that these data reproduce the noise free result, indicated by the thin line.

influence of the noise. After a simple averaging over five adjacent points, the correlation function given by the filled squares is obtained. Clearly, at scales smaller than the averaging time, the exponent is too high, due to correlations introduced by the averaging. At longer time scales an exponent of $\sim$0.43(3) is obtained, which underestimates the true value. Using equation (11) to correct for the noise, we obtain the filled circles. Note the perfect agreement with the noise free correlation function plotted as a thin line. The exponent obtained by fitting the data in the interval $t \in [1, 11]$ is 0.50(2), which reproduces very nicely the ideal result. Note, however, that an underestimation of the noise by 1% leads to an exponent of 0.46, indicating that good knowledge of the strength of the noise is essential for the correction to work.

5 Analysis of experimental magnetic field profiles

Now that we have shown that even very substantial noise can be corrected for by the present method, we apply it to the magnetic field profiles in $YBa_2Cu_3O_{7-x}$ thin films. However, to correct for the noise we first have to determine the noise in our experiments itself. Therefore we now first discuss how to determine the noise.

As follows directly from the second term in equation (6) the noise strength increases with ϕ and thus along the profile. In the following we will show that this ϕ dependence of σ is small. Therefore we discuss 2 cases: Firstly, we determine the noise at zero external field. Secondly, we discuss the case where there is an applied external field, such that a ϕ-gradient is present in the images.

The noise $\sigma_{\phi\approx 0}$ may be determined directly from the experimental ϕ images at zero applied field. To compensate for any irregularities in the indicator layer, the *difference* of two (consecutive) images at zero applied field is taken and divided by $\sqrt{2}$ to give an image for $\phi = 0$ which only contains noise. The standard deviation of such an image gives $\sigma_{\phi\approx 0} = 9.00 \times 10^{-4}$ rad, which is also what is obtained from equation (6) using experimental values for I, K and α. Furthermore, the correlation function *of the noise itself* $C_{noise}(x, 0)$, turns out to be independent of x with a value of $\sigma\sqrt{2}$, thus allowing the use of equation (11), with σ a constant.

However, if there is an applied magnetic field and profiles are present we encounter the problem that the noise σ increases with ϕ and thus along the profile. Fortunately this does not mean that the noise increases with time in the experiment, since the profiles are connected to the front and thus the local ϕ values on the profiles are roughly constant during the whole experiment. Moreover, in order to eliminate a position dependence of the noise we use the noise averaged over the profile for the noise correction procedure. This is justified by the fact that the ϕ-dependent contribution to the noise is small (see below). Thus we determine the noise from the standard deviation σ of the *difference* of values in *the region covered by the profiles* between two consecutive images divided by $\sqrt{2}$. In this manner we find averaged over all differences between consecutive images $\sigma = 9.24(27) \times 10^{-4}$ rad. This shows that the ϕ dependence of σ is small.

A typical example of the fluctuations, $b(x)$, of a measured slope-free profile is shown in Figure 5. In Figure 6 the corresponding spatial correlation functions for all profiles are shown, both uncorrected and noise-corrected using equation (11) and the value of σ determined above. As can be seen, in the uncorrected case (open circles) there is no clear power law behavior and the exponent α is severely underestimated. In the noise-corrected data (full circles), power law behavior is obtained allowing an accurate determination of $\alpha = 0.75(6)$ from a weighted fit in the interval

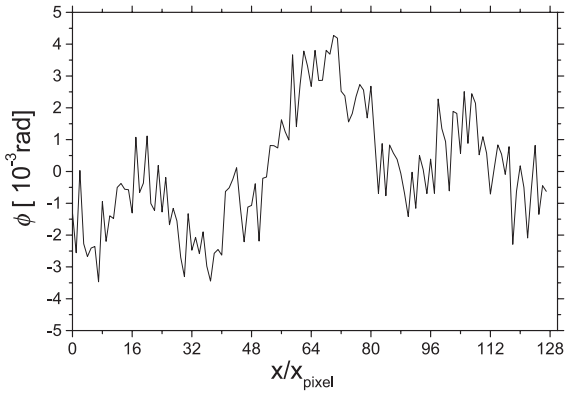

Fig. 5. A typical example of the height fluctuations of a slope-free magnetic field profile as determined from a MO image such as Figure 1. In total more than 10^5 of these profiles were analyzed.

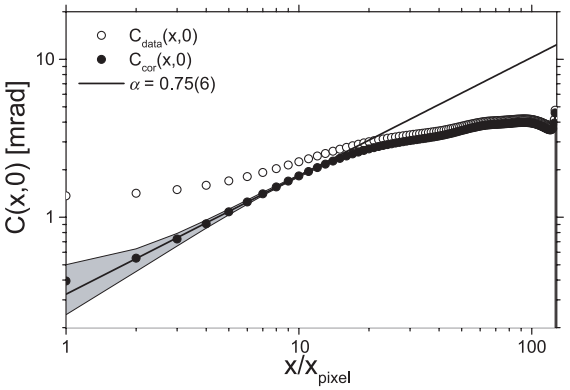

Fig. 6. The spatial behavior of the two-point correlation function for the magnetic field profiles. The open circles show $C_{data}(x,0)$, calculated from the uncorrected noisy data and yielding a roughness exponent of $\alpha = 0.40(5)$. The filled circles show $C_{cor}(x,0)$ calculated from equation (11). Clearly, power law scaling is obtained yielding an exponent of $\alpha = 0.75(6)$, indicated by the black line. The shaded area indicates the error margin in the correction scheme corresponding to 1 standard deviation in the noise.

$x/x_{pixel} \in [1,11]$. The influence of the error in the noise determination on $C_{cor}(x,0)$ is shown by the shaded area.

For the temporal analysis extra care must be taken since the profiles are connected to the fronts. The noise in the images generates a statistical error with width δ in the determination of the front position. Since we fix the profiles to the front, profiles at different times are connected to different fronts and the temporal correlation function has an extra error (noise contribution) due to the uncertainty in the front position. Since the slope of the profiles projects the noise in the profile height in the x-direction, we estimate δ from σ divided by the averaged local slope s at the front, hence $\delta = \sigma/s$. This implies that in stead of the true $C(0,t)$, one effectively calculates $C_{calc}(0,t) = \sqrt{C^2(0,t) + 2C^2(\delta,0)}$. Here, $C(\delta,0)$ is determined from the noise corrected spatial correlation function. Thus for the intrinsic width correction of $C(0,t)$, the noise σ in equation (11) must be replaced by $\sqrt{\sigma^2 + C^2(\delta,0)}$. With

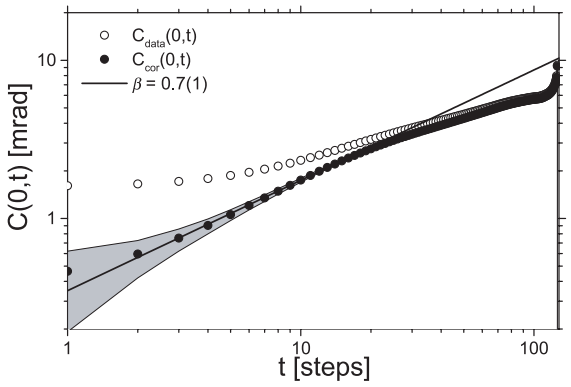

Fig. 7. The temporal behavior of the two-point correlation function for the magnetic field profiles. The open circles show $C_{data}(0,t)$, calculated from the uncorrected noisy data and yielding a growth exponent $\beta = 0.30(5)$. The filled circles show $C_{cor}(0,t)$ calculated from equation (11) using an effective noise value of $10.9(4) \times 10^{-4}$ rad. Clearly, power law scaling is obtained yielding an exponent of $\beta = 0.7(1)$, indicated by the black line. The shaded area indicates the error margin in the correction scheme corresponding to 1 standard deviation in the noise.

$C(\delta,0) = 5.7 \times 10^{-4}$ rad, this yields an effective noise value of $10.9(4) \times 10^{-4}$ rad in $C(0,t)$.

In Figure 7, the time correlation functions are shown uncorrected (open circles) and corrected (filled circles). It can be seen that without correcting for the noise, the determination of the exponent underestimates the true value. As can be seen, in the noise-corrected data power law behavior is observed with an exponent of $\beta = 0.7(1)$ from a weighted fit in the interval $t \in [1,17]$. The influence of the error in the noise determination on $C_{cor}(0,t)$ is shown by the shaded area.

Note that in both space and time, the corrected data still have a small upturn at small scales which may be due to a slight underestimation of the experimental noise. However, as indicated by the shaded area, the deviation is smaller than the error bars. Also the possible effect on α and β is well within the errorbars of these exponents. Note also that the curves shown in Figures 6 and 7 were corrected using the experimental σ and thus σ is not a fitting parameter to equation (11).

6 Discussion

In conclusion, noise in experimental systems may hamper an accurate determination of the self-affine properties of interfaces such as the growth and roughness exponents. In order to correct the correlation functions for the presence of noise in the experimental data an accurate determination of the noise strength is necessary. We describe and test a noise removal procedure on an artificial random walk model with added noise and show that the analytic value of the exponent can be recovered. Furthermore, we investigate the self-affine properties of the magnetic field profiles in $YBa_2Cu_3O_{7-x}$ thin films. We

show that without correction, the presence of noise leads to an underestimation of both the growth and roughness exponent. Measuring the experimental noise and correcting the correlation functions for its presence, we find for the magnetic flux profiles $\alpha = 0.75(6)$ for the roughness exponent and $\beta = 0.7(1)$ for the growth exponent. Note that these values are different from results reported earlier [18], where no noise correction was applied.

Thus magnetic vortices in superconductors fall well into the category of roughening systems with quenched disorder, such as fluid flow in porous media [2,3], mountain ranges [9], wet granular piles [9], and bacterial colony growth [1]. All these systems show roughness exponents of $\alpha \simeq 0.8$. In systems where the growth exponent was determined as well, it is also in the same range as that determined here, varying from $\beta = 0.65$ (fluid flow [4]) to $\beta = 0.85$ (wet granular piles [9]).

We would like to thank Jan Rector for the samples. This work was supported by FOM (Stichting voor Fundamenteel Onderzoek der Materie), which is financially supported by NWO (Nederlandse Organisatie voor Wetenschappelijk Onderzoek).

References

1. T. Vicsek, M. Cserző, V.K. Horváth, Physica A **167**, 315 (1990)
2. S. He, G.L.M.K.S. Kahanda, P. Wong, Phys. Rev. Lett. **69**, 3731 (1992)
3. M.A. Rubio, C.A. Edwards, A. Dougherty, J.P. Gollub, Phys. Rev. Lett. **63**, 1685 (1989)
4. V.K. Horváth, F. Family, T. Vicsek, J. Phys. A **24**, 25 (1991)
5. J. Kertész, V.K. Horváth, F. Weber, Fractals **1**, 67 (1992)
6. J. Zhang, Y.-C. Zhang, P. Alstrøm, M.T. Levinsen, Physica A **189**, 383 (1992)
7. M. Myllys, J. Maunuksela, M.J. Alava, T. Ala-Nissila, J. Timonen, Phys. Rev. Lett. **84**, 1946 (2000)
8. M. Myllys, J. Maunuksela, M. Alava, T. Ala-Nissila, J. Merikoski, J. Timonen, Phys. Rev. E **64**, 36101 (2001)
9. A. Czirók, E. Somfai, T. Vicsek, Phys. Rev. Lett. **71**, 2154 (1993)
10. A. Malthe-Sørenssen, J. Feder, K. Christensen, V. Frette, T. Jøssang, Phys. Rev. Lett. **83**, 764 (1999)
11. C.M. Aegerter, R. Günther, R.J. Wijngaarden, Phys. Rev. E **67**, 51306 (2003)
12. E. Moro, Phys. Rev. Lett. **87**, 238303 (2001)
13. J. Kertész, D.E. Wolf, J. Phys. A **21**, 747 (1988)
14. A.-L. Barabási, H.E. Stanley, *Fractal Concepts in Surface Growth* (Cambridge University Press, 1995)
15. L.A. Dorosinskii, M.V. Indenbom, V.I. Nikitenko, Y.A. Ossipyan, A.A. Polyanskii, V.K. Vlasko-Vlaskov, Physica C **203**, 149 (1992)
16. J.M. Huijbregtse, B. Dam, J.H. Rector, R. Griessen, J. Appl. Phys. **86**, 6528 (1999)
17. R.J. Wijngaarden, K. Heeck, M. Welling, R. Limburg, M. Pannetier, K. van Zetten, V.L.G. Roorda, A.R. Voorwinden, Rev. Sci. Instrum. **72**, 2661 (2001)
18. M.S. Welling, C.M. Aegerter, R.J. Wijngaarden, Europhys. Lett. **61**, 473 (2003)